Optimal Fiber Link Fault Decision for Optical 2D Coding-Monitoring Scheme in Passive Optical Networks

Min Zhu, Jiao Zhang, Dongpeng Wang, and Xiaohan Sun

***Abstract*—Several fiber-fault monitoring schemes based on traditional OTDR technique have been proposed for monitoring fiber links in passive optical networks (PONs). However, in a tree-topology PON, it is difficult for network managers to distinguish which fiber link the fault occurs in. Thus, some schemes based on an optical coding technique have been proposed to overcome the optical time-domain reflectometry disadvantages in monitoring point-to-multipoint networks. In this paper, we develop a mathematical model for an optical 2D coding-monitoring system in PONs which includes three modules: detection pulse generator, optical encoding and transmission, and optical decoding and fault identification. We also analyze the correlation distance expression and interference probability with partial overlap between any two 2D codes. In addition, we derive close-form expressions for P_D (detection probability) and P_{FA} (false-alarm probability) by analyzing the target signal, interference, and all possible noises, which are used to calculate optimal decision probability. The system performance in terms of signal-to-noise ratio, signal-to-interference ratio (SIR), and the optimal decision probability are investigated with different system parameters such as client separation distance, network size, transmitted pulse width, and transmitted pulse power. The extensive simulation results show that the optimal transmitted pulse width is $T_C \approx 1$ ns and the SIR is to a lower bound of ~21 dB. It is concluded that suitable system variables can be chosen optimally to facilitate the optimal decision.**

***Index Terms*—Normalized threshold current (NTC); Optimal decision probability (ODP); Partial interference; Signal-to-interference ratio (SIR); Signal-to-noise ratio (SNR).**

I. Introduction

Passive optical networks (PONs) have been considered by network operators to be the best choice of next-generation broadband access solutions because they offer huge bandwidth, excellent security, and easy upgradability [1]. It was reported that the majority of the operation and maintenance expense is on monitoring link faults [2,3]. Therefore, research on how to effectively identify the fiber faults that arise from multiple branches of PONs can help to reduce the capital and operation expenditures for both the network provider and customers. However, the primary challenge in fiber-fault monitoring is to identify a specific broken fiber branch from multiple branches of a PON [4–11].

A variety of solutions have been proposed to adapt the standard optical time-domain reflectometry (OTDR) to a PON [4–7]. As is well known, standard OTDR, based on Fresnel reflections and Rayleigh backscattering, is generally used to monitor point-to-point links rather than point-to-multipoint (PMP) links in PONs; this is because the backscattering signal of each branch in a PMP network is partially masked by that of the other branches. It is difficult for a central office (CO) network manager to distinguish the events in a tree-architecture PON. As a modified solution in [7], a tunable OTDR is used along with wavelength-selective isolators in the remote node (RN) to distinguish each branch. Furthermore, these solutions are impractical due to their limited network size and higher system complexity.

Thus, some optical coding schemes based on modified optical code division multiplexing have been proposed for centralized optical fiber in-service monitoring systems. These schemes overcome the OTDR PMP shortcomings and offer a promising solution for monitoring in a large number of PON users [8–11]. A modified 1D optical periodic coding (PC) scheme has been proposed and demonstrated experimentally using fiber Bragg grating (FBG) encoders [8,9]. Regarding this scheme, the correlation distance of the PC is large in a high-capacity PON, which results in severe multiple-customer interference. In addition, each subscriber has a specially designed optical encoder, which is made of a pair of FBGs with different fiber length between them. The reflectivity of the first FBG is optimized to be 38% and the reflectivity for the second FBG is fixed to be 100% [8]. This encoder-coding scheme increases the difficulty of manufacture. Moreover, the service capacity (number of customers) of this scheme is still limited. In our previous work [10,11], a centralized optical monitoring scheme in a PON is proposed based on the 2D optical frequency hopping/periodic coding scheme with a network recognition algorithm that converts the decoding operation into an electronic field. As experimentally demonstrated, the results show that the proposed scheme achieves smaller correlation distance and larger capacity than the PC scheme. The status of the fiber link in a PON can be monitored by the implementation of the network-recognition

Manuscript received November 30, 2015; revised January 26, 2016; accepted January 26, 2016; published February 17, 2016 (Doc. ID 254742).

The authors are with the National Research Center for Optical Sensing/Communications Integrated Networking, the School of Electronic Science and Engineering, Southeast University, Nanjing 210096, China (e-mail: minzhu@seu.edu.cn).

http://dx.doi.org/10.1364/JOCN.8.000137

1943-0620/16/030137-11$15.00/0

algorithm [11]. However, these previous works just deal with the fiber fault identification and do not account for the evaluations of monitoring signal quality and optimized design of fiber fault decisions. We note that, for a network manager, any mistaken decision in the status evaluation of a distribution drop fiber (DDF) link would result in non-negligible operational expenditure.

In this paper, we first theoretically analyze the decision performance of the 2D coding-monitoring method in PONs by developing a mathematical model where interference and noise sources are involved. We derive the expression of the correlation distance and partial interference probability from the developed model. Our primary analysis focuses on two decision-performance metrics: 1) optimal decision threshold (ODT, i.e., a value range of normalized threshold current) and 2) optimal decision probability (ODP). Using the evaluation results of ODT and ODP performance, we can obtain the optimal value range of transmitted pulse power and transmitted pulse widths. Hence, the efficiency and accuracy of fiber fault identification is improved greatly and the overall cost of the PON monitoring system is reduced by optimally choosing suitable system variables.

The rest of this paper is organized as follows: in Section II, we first describe the principle of the 2D coding-monitoring system and develop a mathematical model for the monitoring system. Then we derive the optimal decision probability expression in Section III. We present simulation conditions and evaluate different performance metrics of the PON monitoring scheme in Section IV. Finally, the conclusion is drawn in Section V.

II. System Mathematical Model

As illustrated in Fig. 1, this system model contains three modules: detection pulse generator (DPG), optical encoding and transmission (OET), and optical decoding and fault identification (ODFI). The DPG module generates a U-band probe pulse $Q_{\text{in}}(t,\lambda)$ with the duration of T_C and the power of P_S. In this paper, we focus on the monitoring system mathematical model and performance analysis; hence, the principle and structure description of the encoder and decoder is out of the scope of the paper and can be referenced in our previous papers [10,11].

A. System Response Function for OET Module

In the OET module, the probe pulse is transmitted through a circulator and a section of feeder fiber (FF) to a RN, where it is split into N sub-pulses by a $1{:}N$ passive splitter. Every sub-pulse travels through the DDF to the corresponding optical network unit (ONU) and is 2D-coded into a sub-pulse sequence by an optical encoder at the DDF ends before ONUs. The encoder is transparent to C-band data signals, and reflects the encoded sub-pulse sequence in the U-band for link monitoring to the CO. In this paper, the 2D optical orthogonal codes (OOCs) are represented by a family of $(F, M, w, \lambda_a, \lambda_c)$, where F is the code length, M is the number of wavelengths, w is code weight, and $\lambda_a = 1$ and $\lambda_c = 1$ are maxima of auto- and cross-correlation values, respectively [12]. The optical 2D-encoder function expression for ONU-k can be defined as

$$Ec_k(t,\lambda) = \sum_{i=1}^{w} \alpha_e \delta(t - \tau_{k,i}, \lambda_{k,i}), \tag{1}$$

where α_e denotes the encoder insertion loss, $\lambda_{k,i}$ is the center wavelength of the ith reflected pulse and $\tau_{k,i}$ is the delay, and δ is the Dirac delta function. We assume that the number of Bragg wavelengths of each optical encoder is equal to the code weight.

Assuming the monitoring system is a linear system, the roundtrip impulse response of the OET module in Fig. 1 is expressed as follows:

$$h_{\text{OCT}}(t,\lambda) = \underbrace{\frac{1}{K}}_{\text{Splitter}} \sum_{k=1}^{K} \xi_k \cdot \underbrace{h_{\text{FF}}(t) * h_{\text{DDF}_k}(t)}_{\text{forward path}} * E_{C_k}(t,\lambda) * \underbrace{h_{\text{DDF}_k}(t) * h_{\text{FF}}(t)}_{\text{backward path}}, \tag{2}$$

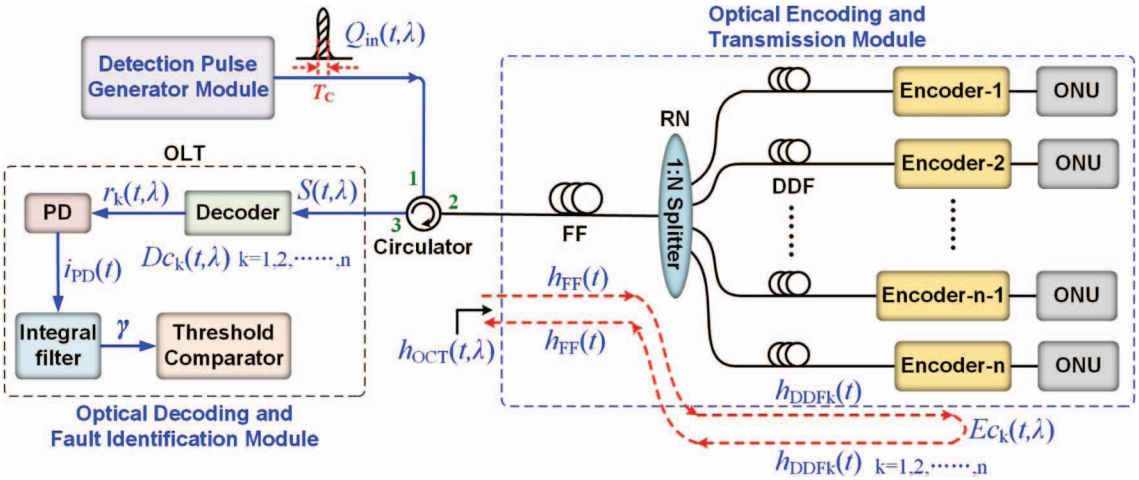

Fig. 1. Diagram of the fiber link monitoring system model based on 2D coding technique in a PON.

$$h_{\mathrm{FF}}(t) = e^{-\alpha_a l_{\mathrm{FF}}/2}\delta(t - l_{\mathrm{FF}}/c), \tag{3}$$

$$h_{\mathrm{DDF}_k}(t) = e^{-\alpha_a l_{\mathrm{DDFk}}/2}\delta(t - l_{\mathrm{DDF}_k}/c), \tag{4}$$

where Eqs. (3) and (4) are the impulse response of the FF and DDFs considering a delay and attenuation model, respectively; c is the light speed in fiber; $*$ denotes convolution operation; and α_a is the fiber attenuation coefficient. We assume that the FF and the DDF have identical α_a. $\xi_k \in \{0, 1\}$ means different status of the DDF_k. Specifically, when DDF_k is broken, $\xi_k = 0$; when DDF_k is healthy ($\xi_k = 1$), the transmitted pulse is coded and reflected back to the ODFI module in the CO. The factor $1/K$ shows the total attenuation due to the passive splitter at the RN in upstream and downstream paths. Then the roundtrip signal as an input of the ODFI module is expressed to be

$$S(t, \lambda) = Q_{\mathrm{in}}(t, \lambda) * h_{\mathrm{OCT}}(t, \lambda). \tag{5}$$

B. Decoding Operation in the ODFI Module

The ODFI module in the CO consists of a correlation decoder, photodetector (PD), integral filter, and threshold comparator. The decoded monitoring pulses are converted into electrical signal by the PD and then go through the integral filter to the threshold comparator, which extracts status information about each fiber link according to the autocorrelation peak [8].

As an input of the ODFI module, the signal $S(t, \lambda)$ passes through the decoder, so we obtain the decoded optical signal as follows:

$$r_i(t, \lambda) = Dc_i(t, \lambda) * S(t, \lambda) = \xi_i A_i(t, \lambda) + \sum_{k=1, i\neq k}^{K} \xi_k B_{i,k}(t, \lambda), \tag{6}$$

$$Dc_i(t, \lambda) = \sum_{j=1}^{w} \alpha_d \delta(t - (T - T_C - \tau_{i,j}), \lambda_{i,j}). \tag{7}$$

In Eq. (6), the first term is the desired monitoring signals for the ith encoder with its decoder; the second term is the interference signals for the kth encoder with the ith decoder. $Dc_i(t, \lambda)$ is the impulse response function of the ith correlation decoder as shown in Eq. (7), where α_d denotes the decoder insertion loss and $T - \tau_{k,i}$ is the delay term. The decoder has autocorrelation peak at the time interval $[T - T_C, T]$ and T is the repetition interval. The desired $A_i(t, \lambda)$ and interference $B_{i,k}(t, \lambda)$ signal expression can be obtained as follows by substituting the $S(t, \lambda)$ expression into Eq. (6):

$$A_i(t, \lambda) = \alpha_L \frac{1}{K} Q_{\mathrm{in}}(t, \lambda) * h_{\mathrm{FF}}(t) * h_{\mathrm{DDF}_i}(t) * Ec_i(t, \lambda) * h_{\mathrm{DDF}_i}(t) * h_{\mathrm{FF}}(t) * Dc_i(t, \lambda), \tag{8}$$

$$B_{i,k}(t, \lambda) = \alpha_L \frac{1}{K} Q_{\mathrm{in}}(t, \lambda) * h_{\mathrm{FF}}(t) * h_{\mathrm{DDF}_k}(t) * Ec_k(t, \lambda) * h_{\mathrm{DDF}_k}(t) * h_{\mathrm{FF}}(t) * Dc_i(t, \lambda). \tag{9}$$

Using Eqs. (1)–(4) in conjunction with Eqs. (8) and (9), we can obtain detailed desired and interference signal expression, respectively, as follows:

$$A_i(t, \lambda) = \frac{\alpha_L \alpha_e \alpha_d e^{-\alpha_a l_i}}{K} \sum_{u=1}^{w} Q_{\mathrm{in}}\left(t - \left(T - T_c + 2\frac{l_i}{c}\right), \lambda_{i,u}\right), \tag{10}$$

$$B_{i,k}(t, \lambda) = \frac{\alpha_L \alpha_e \alpha_d e^{-\alpha_a l_k}}{K} \sum_{v=1}^{w} \sum_{u=1}^{w} Q_{\mathrm{in}}\left(t - \left(T - T_c - \tau_{i,u} + \tau_{k,v} + 2\frac{l_i}{c}\right), \lambda_{i,u}\right). \tag{11}$$

The factor α_L denotes the total attenuations, including the connectors, splitter, circulator, etc., in the monitoring system and $l_k = l_{\mathrm{FF}} + l_{\mathrm{DDF}_k}$ is the length of the FF and DDFs.

The decoded monitoring pulses are converted into electrical signal by the PD with a gain G. By using a square law model, the photocurrent can be expressed as

$$i_{\mathrm{PD}}(t) = G|r_i(t, \lambda)|^2 + i_n(t), \tag{12}$$

where the noise term $i_n(t)$ will be discussed in Subsection II.D.

In Fig. 1, after being sampled by the integral filter signal, the decision variable γ is obtained and then compared to a threshold value. The optimal decision can be realized via the optimally designed threshold value. Detection takes place only during an observation window of length T_C (one optical pulse width). The decision variable γ can be formulated as

$$\gamma = \frac{1}{T_C} \cdot \int_{t\in T_{\mathrm{obs}}} i_{\mathrm{PD}}(t)\mathrm{d}t = \mu_{\mathrm{sig}} + \mu_{\mathrm{int}} + \gamma_n, \tag{13}$$

where the desired signal μ_{sig} and the interference contribution μ_{int} can be derived as follows:

$$\mu_{\mathrm{sig}} = G\alpha_{\mathrm{Total}}\xi_i e^{-2\alpha_a l_i} \sum_{n=1}^{w} \frac{1}{T_c} \int_{t\in T_C} |Q_{\mathrm{in}}(t_i, \lambda_{i,u})|^2 \mathrm{d}t = G\alpha_{\mathrm{Total}}\xi_i e^{-2\alpha_a l_i} w P_s, \tag{14}$$

$$\mu_{\mathrm{int}} = G\alpha_{\mathrm{Total}} \sum_{k=2}^{K} \rho_k e^{-2\alpha_a l_k} \sum_{n=1}^{w} \frac{1}{T_c} \int_{t\in T_C} |Q_{\mathrm{in}}(t_k, \lambda_{i,u})|^2 \mathrm{d}t = G\alpha_{\mathrm{Total}} \sum_{k=2}^{K} \rho_k e^{-2\alpha_a l_k} P_s, \tag{15}$$

where the factor ρ is the sub-pulse interference probability, which is discussed later in the following sections. P_s is the power of the 2D-OOC signal including w sub-pluses.

C. Analyses of Partial Interference Probability

As illustrated in Fig. 2(a), when the distance difference $(l_2 - l_1)$ between the target decoder D_1 and another decoder D_2 is larger than the distance of a 2D sub-pulse sequence (i.e., the distance difference between the first and the last sub-pulses in a code sequence) $c \times FT_C/2$, the decoded signal reflected by D_2 cannot fall into the correlation distance of the target 2D-OOC signal, and hence there are no interference components. On the contrary, while the distance difference $(l_i - l_1)$ between D_i and D_1 is smaller than $c \times FT_C/2$, the partial sub-pulses will overlap and contribute to interference with each other. Therefore, we define the correlation distance (CD) as follows:

$$l_{\mathrm{CD}} = c \times FT_C/2. \tag{16}$$

In traditional OCDMA theory, to analyze the interference probability ρ between two codes, it is assumed that the code weight w (i.e., sub-pulse) of 2D OOCs is a uniform distribution statistic for the sake of mathematical convenience. It should be noted that the two codes overlap almost completely in the time domain. The interference between two codes indicates that one of the sub-pulses (i.e., a binary one) in a 2D code word coincides with a sub-pulse in another 2D code word. For the family of 2D OOCs $(F, M, w, \lambda_a, \lambda_c)$ with the maximum cross-correlation value of 1 (i.e., $\lambda_c = 1$), the one-hit probability is $\rho = w^2/MF$ [13].

However, in the 2D OOC-based PON monitoring system, due to the different lengths of DDFs, any two 2D codes (i.e., monitoring signals) from the different branches would partially overlap in the time domain as shown in Fig. 2. We assume that two branches have distance difference Δl $(\Delta l > 0)$. In Fig. 2(b), the C_1 overlaps partially with C_i and C_j, respectively. The partial overlap ratio of two 2D-OOC codes can be calculated to be $(1 - \Delta l/l_{\mathrm{CD}})$. Reasonably, only the overlap part of the two 2D-OOC codes can contribute to interference. Hence, we can get the partial interference probability ρ as follows:

$$\rho = \frac{w^2}{MF} \cdot \left(1 - \frac{\Delta l}{l_{\mathrm{CD}}}\right). \tag{17}$$

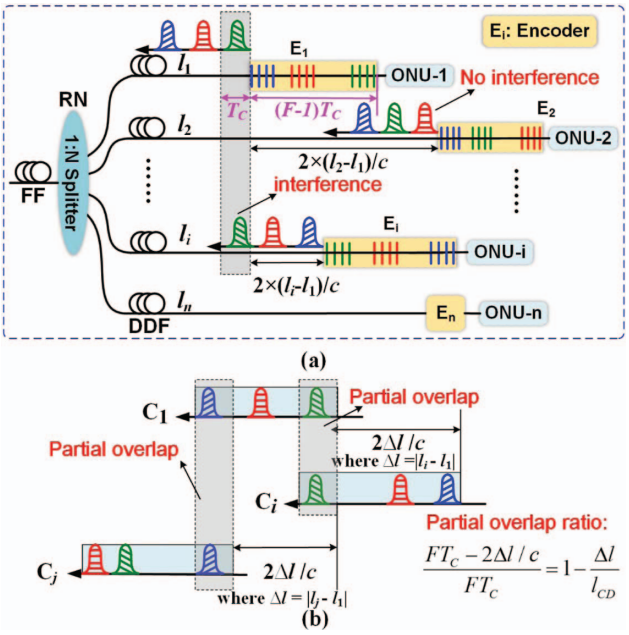

Fig. 2. (a) Principle of correlation distance. (b) Partial overlap ratio between C_i or C_j and C_1, respectively.

D. Definition of SNR and SIR

From Eq. (12), the total output photocurrent after the PD includes not only electrical signals but also all possible noise sources in this mathematical model. It can be expressed as

$$i_{\mathrm{PD}}(t) = G|r_i(t,\lambda)|^2 + i_{\mathrm{BN}}(t) + i_{\mathrm{SN}}(t) + i_{\mathrm{DN}}(t) + i_{\mathrm{TN}}(t). \tag{18}$$

The terms $i_{\mathrm{BN}}(t)$, $i_{\mathrm{SN}}(t)$, $i_{\mathrm{DN}}(t)$, and $i_{\mathrm{TN}}(t)$ denote current noise sources: beat noise (BN), shot noise (SN), dark current noise (DN), and thermal noise (TN) of the receiver [14]. Assuming that all the noise components are uncorrelated, the total noise power can be simply calculated by summing all noise component powers (BN, SN, DN, and TN). The random variable γ_n in Eq. (13) is zero mean and its conditional power $\sigma_n^2 = \sigma_{\mathrm{BN}}^2 + \sigma_{\mathrm{SN}}^2 + \sigma_{\mathrm{DN}}^2 + \sigma_{\mathrm{TN}}^2$. Without loss of generality, γ_n is modeled to be Gaussian. The conditional power of these noises is defined, respectively, as [14–16]

$$\delta_{\mathrm{BN}}^2 = 2\xi_i \cdot \beta(1+\varsigma) \cdot (\alpha_T G P_s)^2 \cdot we^{-2\alpha_a l_i} \sum_{k=2}^{K} \rho_k e^{-2\alpha_a l_k}, \tag{19}$$

$$\delta_{\mathrm{SN}}^2 = qG(1+\varsigma)(\mu_{\mathrm{sig}} + \mu_{\mathrm{int}})B_e, \tag{20}$$

$$\delta_{\mathrm{DN}}^2 = qI_{\mathrm{DN}}(t)B_e, \tag{21}$$

$$\delta_{\mathrm{TN}}^2 = N_{\mathrm{TN}}B_e. \tag{22}$$

With Eq. (13), we consider the following SNR expression, i.e., the ratio of the expectation of the signal power μ_{sig}^2 to the average of all known noise powers δ_n^2 [17],

$$\mathrm{SNR} \overset{\mathrm{def}}{=} \frac{E(\mu_{\mathrm{sig}}^2)}{E(\delta_n^2)} = \frac{E(\mu_{\mathrm{sig}}^2)}{E(\delta_{\mathrm{BN}}^2 + \delta_{\mathrm{SN}}^2 + \delta_{\mathrm{DN}}^2 + \delta_{\mathrm{TN}}^2)}. \tag{23}$$

The SIR is defined as the ratio of the expectation of signal power μ_{sig}^2 to the expectation of interference power μ_{int}^2, using Eqs. (14) and (15):

$$\mathrm{SIR} \overset{\mathrm{def}}{=} \frac{E(\mu_{\mathrm{sig}}^2)}{E(\mu_{\mathrm{int}}^2)}. \tag{24}$$

In the following section, we will first evaluate the system performance of the SNR and SIR in detail. Then, our primary analysis focuses on the optimal decision probability

to realize optimal fault decision and reduce monitoring cost.

III. Optimal Decision Probability

For any PON monitoring solution, the efficiency and accuracy of fiber fault identification are of utmost importance. On the one hand, claiming a fiber link fault when no link fault exists results in unnecessary operational expenditure. On the other hand, if the CO network manager fails to detect a fiber link fault, it would bring about user complaints and dissatisfaction. Hence, the detection probability (P_D) and false-alarm probability (P_{FA}) are extremely significant. The detection probability P_D is defined as the probability of correctly declaring a fiber link faulty, i.e., $P_D = \Pr(\gamma(\zeta = 0) \le \mu)$, where μ is the threshold current of the comparator depicted in Fig. 3. Likewise, the false alarm probability P_{FA} is the probability of declaring a fiber link faulty while it is healthy, i.e., $P_{\mathrm{FA}} = \Pr(\gamma(\zeta = 1) \le \mu)$.

At first, we analyze signal sources according to several different cases of fiber link status illustrated in Table I. As we know, the BN analysis is complex because it consists of three noise components: signal-to-signal beating (SSB), signal-to-interference beating (SIB), and interference-to-interference beating (IIB) [15,16]. When the target fiber link is healthy ($\zeta = 1$), all the μ_{sig} (desired signal), μ_{int} (interference signal), and four kinds of noise sources (i.e., BN, SN, DN, TN) exist. We have discussed and derived the expressions of the μ_{sig} and μ_{int} in Section II. The SSB component can be eliminated because the electrical filter can remove the beating noise among the sub-pulses with different center wavelengths in an optical 2D-coding signal. Generally the IIB is much smaller than the SIB, so we can approximately obtain the expression $\sigma^2_{\mathrm{BN}} \approx \sigma^2_{\mathrm{SIB}}$. On the contrary, while the target fiber link is broken ($\zeta = 0$), no desired signal μ_{sig} exists and hence the beating component is also nonexistent ($\sigma^2_{\mathrm{BN}} \approx \sigma^2_{\mathrm{SIB}} = 0$), but the μ_{int} and the other three kinds of noise sources (i.e., SN, DN, TN) do still exist.

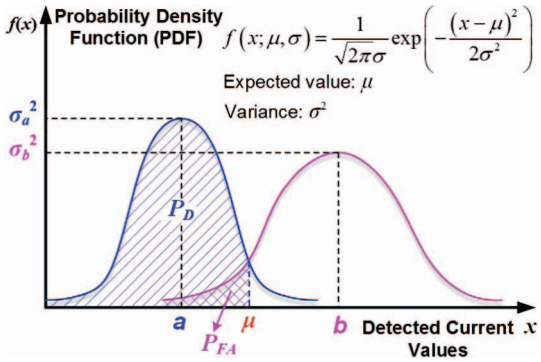

Fig. 3. Two Gaussian probability density functions for P_D and P_{FA}, where μ is the optimal decision threshold.

To obtain better performance, we assume that a coherent source (laser) is used in the PON monitoring system. Therefore, there is no severe relative intensity noise (RIN), i.e., $\sigma^2_{\mathrm{RIN}} = 0$. Note that, if broadband source (BBS) is employed in the system, it would suffer from significant RIN due to the spectrum slicing of the BBS source [16].

As illustrated in Fig. 3, the decision variable γ with expected value μ_n and variance σ^2 is assumed to be Gaussian. From the noise source analysis just presented, when the target fiber link is broken ($\zeta = 0$), no coded signal for the corresponding ONU is received and hence $a = \mu_a = E\{\mu_{\mathrm{int}}\}$, $\sigma_a^2 = \sigma^2_{\mathrm{SN}} + \sigma^2_{\mathrm{DN}} + \sigma^2_{\mathrm{TN}}$. When the fiber link is healthy ($\zeta = 1$), the transmitted pulse is coded and reflected back to the CO, and thus $b = \mu_b = E\{\mu_{\mathrm{sig}} + \mu_{\mathrm{int}}\}$, $\sigma_b^2 = \sigma^2_{\mathrm{BN}} + \sigma^2_{\mathrm{SN}} + \sigma^2_{\mathrm{DN}} + \sigma^2_{\mathrm{TN}}$. Therefore the P_D and P_{FA} are defined, respectively, as follows:

$$P_D = \frac{1}{\sqrt{2\pi}\sigma_a} \cdot \int_{-\infty}^{\mu} e^{\frac{-(x-a)^2}{2\sigma_a^2}} \mathrm{d}x, \tag{25}$$

$$P_{\mathrm{FA}} = \frac{1}{\sqrt{2\pi}\sigma_b} \cdot \int_{-\infty}^{\mu} e^{\frac{-(x-b)^2}{2\sigma_b^2}} \mathrm{d}x. \tag{26}$$

For easy reference, we will calculate a relative threshold value. We normalize threshold current based on the current of the detected signal as

TABLE I
Signal Source Analysis According to Fiber Status

Signal Source	$\zeta = 1$ (Fiber Healthy)	$\zeta = 0$ (Fiber Broken)
μ_{sig}, Desired signal	Existing	No existing
μ_{int}, Interference signal	Existing	Existing
σ^2_{BN}, Beat noise	Existing	No existing
σ^2_{SN}, Shot noise	Existing	Existing
σ^2_{DN}, Dark current	Existing	Existing
σ^2_{TN}, Thermal noise	Existing	Existing
σ^2_{RIN}, Relative intensity noise	No existing	No existing
a, Expected value	–	$E\{\mu_{\mathrm{int}}\}$
σ_a^2, Variance	–	$\sum \sigma_i^2$, $i \in \{\mathrm{SN}, \mathrm{DN}, \mathrm{TN}\}$
b, Expected value	$E\{\mu_{\mathrm{sig}} + \mu_{\mathrm{int}}\}$	–
σ_b^2, Variance	$\sum \sigma_i^2$, $i \in \{\mathrm{BN}, \mathrm{SN}, \mathrm{DN}, \mathrm{TN}\}$	–

$$i = \frac{\mu - a}{b - a}, \qquad (0 \le i \le 1). \tag{27}$$

For a desired PON monitoring system, we strive to get as high P_D value and as low P_{FA} value as possible. Therefore, the ODP value in our simulation is defined to be $P_{\mathrm{ODP}} = P_D - P_{\mathrm{FA}}$. Using Eqs. (25) and (26), we obtain

$$P_{\mathrm{ODP}} = \frac{1}{\sqrt{2\pi}\sigma_a} \cdot \int_{-\infty}^{\mu} e^{\frac{-(x-a)^2}{2\sigma_a^2}} \mathrm{d}x - \frac{1}{\sqrt{2\pi}\sigma_b} \cdot \int_{-\infty}^{\mu} e^{\frac{-(x-b)^2}{2\sigma_b^2}} \mathrm{d}x. \tag{28}$$

Finally, there exists a decision threshold current μ, where the optimal decision probability P_{ODP} reaches its maximum value. We can get this μ value by solving Eq. (28) as follows:

$$\begin{aligned} \mu &= \frac{B - \sqrt{B^2 - 4AC}}{2A}, \\ A &= \sigma_b^2 - \sigma_a^2, \; B = 2a\sigma_b^2 - 2b\sigma_a^2, \\ C &= a^2\sigma_b^2 - b^2\sigma_a^2 - 2\sigma_a^2\sigma_b^2 \ln(\sigma_b/\sigma_a). \end{aligned} \tag{29}$$

Based on this analysis, we will study the impact of different system factors (i.e., client separation distance, network size, transmitted pulse width, and transmitted power) on the monitoring system performance and ODP. In the following section, we will present the simulation conditions and performance evaluation.

IV. Performance Evaluation

A. Power Budget and Simulation Conditions

To evaluate the performance of the optical 2D coding-monitoring scheme, a power/loss budget analysis with all network elements in the downstream and upstream is given in Table II. In the analysis, we assume that the output power of the coherent source (laser) is about 4 dBm for the standard single-mode fiber (SMF) in order to remove fiber nonlinearity. The total power losses include an insert loss of 2 dB for the optical circulator, 18 dB insertion loss induced by a 1:64 splitter, 6.3 dB transmission loss for 21 km SMF including FF and DDF, and insertion loss of 2.5 dB for the splice/connector. We assume that the insertion loss is 0 dB for the 2D encoder based on multiple FBGs because the 100% reflectivity of the FBGs theoretically introduces no insertion loss. Consequently, the total loss experienced roundtrip by optical pulses is 57.6 dB.

TABLE II
Power/Loss Budget for DS and US Signals

Element Insertion Loss	DS Signal	US Signal
Transmitted power P_s (dBm)	4	–
Circulator insertion loss (dB)	2	2
1:64 splitter insertion loss (dB)	18	18
$l_f = 20$ km FF SMF loss (dB)	6	6
$l_e = 1$ km DDF SMF loss (dB)	0.3	0.3
Splice/connector loss (dB)	2.5	2.5
Encoder/decoder loss (dB)	0	0
Total insertion loss (dB)	57.6	
Received power (dBm)	−53.6	

Considering a transmitted power of 4 dBm, the received power is −53.6 dBm. In the next simulation, we will analyze the effect of transmitted power on the performance of the monitoring system.

Table III lists some simulation values, including all noise sources just analyzed. We consider a family of 2D OOC codes with $[F = Kw(w-1)+1,\ M = w,\ w = 4,\ \lambda_a = 1,\ \lambda_c = 1]$. To provide a good autocorrelation peak and faintish cross-correlation spikes, we limit the autocorrelation side lobes to one and consider a unitary cross-correlation code family, i.e., $\lambda_a = 1, \lambda_c = 1$, respectively [12]. In order to compensate the loss due to passive elements such as splitter/combiner, we use a high-gain PD with a gain $G = 100$ and excess noise factor of $1 + \varsigma = 2.97$. The l_e is the maximum client separation length (i.e., maximum length of DDFs). Each length of the DDFs is uniformly distributed in $[0, l_e]$. If the value of l_e is larger and the value of network size K is smaller, the client density is smaller. Thus, we can vary the values of l_e and K to simulate different client density. We also assume 0.3 dB/km fiber loss and total loss of 5 dB for splicing and connectors, etc. Moreover, I_{DC} in Eq. (21) for dark current (average current = 160 nA) and N_{TN} in Eq. (22) is used for power spectral density (10^{-26} Amp^2/Hz assumed) [14]. For electrical bandwidth B_e and available optical bandwidth B_O, we have a normalized power equal to β in Eq. (19), where, by definition, $\beta \cong B_e/B_o = 1/(B_o T_C)$ [15,16]. The β is proportional to the inverse of the pulse width. In this paper, the bandwidth of the PD is considered to be larger than the electrical bandwidth. Hence, we do not take the bandwidth limitation of the PD into consideration.

B. SNR and Noise Analysis

In the following simulation, we study the performance of SNR by taking all known noise source and simulation parameters in Table III into consideration. At first, we plot SNR given in Eq. (23) versus the transmitted power P_s in the case of $l_f = 20$ km, $K = 64$, and $T_C = 1$ ns in Fig. 4. It can be observed that for different client separation distance l_e, the SNR gradually increases as the transmitted pulse power P_s improves. In the part of $P_s > 0$ dBm, the SNR

TABLE III
Values Used for Simulation

Parameter and Symbol	Value	Unit
M, Number of wavelength	4	–
w, Code weight	4	–
λ_a, Autocorrelation value	1	–
λ_b, Cross-correlation value	1	–
G, APD Gain	100	–
$1 + \varsigma$, APD excess noise factor	2.97	–
l_e, Maximum separation length	[1,5]	Km
α_a, Fiber attenuation coefficient	0.3	dB/km
I_{DC}, Dark current	160	nA
N_{TN}, Thermal noise power	10^{-26}	Amp^2/Hz
α_L, Total connector/splice loss	5	dB
B_o, Laser line width	10	MHz
B_e, (electrical bandwidth)	$1/T_C$	MHz

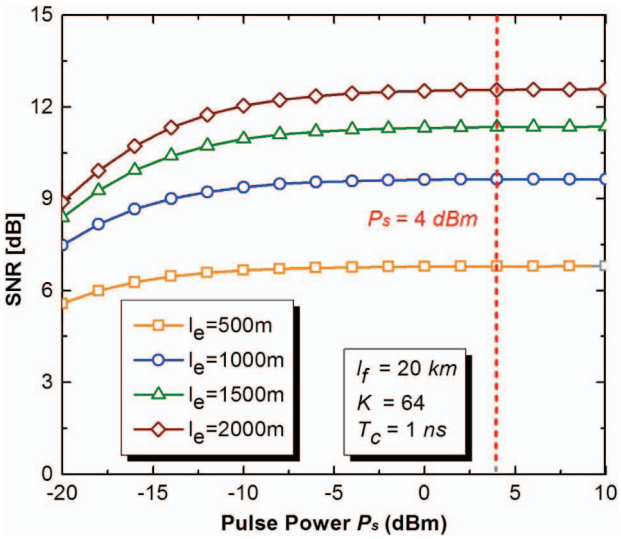

Fig. 4. SNR versus the transmitted pulse power P_s.

almost keeps a stable value and will not obviously change. It should be noted that a higher transmitted pulse power is limited by the fiber nonlinearity. The linear monitoring system is no longer stable for a higher power. Therefore, in our simulation, we consider $P_s = 4$ dBm in order not to induce fiber nonlinearity; in the meantime, the SNR has a desired value.

In Fig. 5, when $l_f = 20$ km, $T_C = 1$ ns, and $P_s = 4$ dBm, we plot SNR curves versus different network size K for different client separation distances l_e. We can observe that the 2D coding-monitoring scheme allows up to 64 clients ($l_e = 1000$ m) to be monitored with a SNR = 9.7 dB. For 128 clients, the SNR decreases to 6.9 dB due to the increase of the client noises. For a given consumer network size (e.g., $K = 64$), as the client separation distance l_e decreases, the SNR value gets smaller because the client noises increase.

We will analyze and compare the share of the different noise components SN, BN, DN, and TN. In the PON link monitoring system, the threshold detection only takes place during T_{obs}, which is equal to a transmitted pulse width ($T_C = T_{\text{obs}}$). Hence, the varied value of T_C would have different effects on all the noise components. Using $l_f = 20$ km, $l_e = 1$ km, $K = 64$, $P_s = 4$ dBm, and other values in Table III, we present all noise sources in the different cases of transmitted pulse width T_C in Fig. 6. We find that the value of SN and BN is about 60 dB larger than DN and TN, and hence we can ignore DN and TN. The SN, DN, and TN show a linearly decreasing trend as the T_C increases because they are proportional to the electrical bandwidth ($B_e = 1/T_C$), as shown in Eqs. (20)–(22). As mentioned in Section III, it can be obtained that $\sigma^2_{\text{BN}} \approx \sigma^2_{\text{SIB}}$. For shorter pulse width, the BN is smaller than SN because the interference is lower. Therefore, when $T_C < 10^{-10}$ s, the SN dominates. As the pulse width increases, leading to higher correlation distance l_{CD} ($l_{\text{CD}} = cFT_C/2$), increasing interference would lead to the higher BN power. Specifically, when $T_C > 10^{-10}$ s, the BN dominates. While T_C is roughly between 10^{-8} and 10^{-7}, the BN reaches a maximum. But, as the pulse width T_C continues to increase, the BN will become decreased because it is inversely proportional to the pulse width T_C as shown in Eq. (19).

In Fig. 7, we give out SNR performance in the cases of different transmitted pulse width T_C and client separation distance l_e, when $l_f = 20$ km, $K = 64$, and $P_s = 4$ dBm. As discussed in Fig. 6, in the case of the narrow pulse width (e.g., $T_C < 10^{-10}$ s), the SN dominates and linearly decreases as the T_C increases. Hence, we can observe that the SNR presents a linearly increasing trend. In the left inset, there are some subtle differences of SNR values due to the different interferences with different l_e. As the pulse width increases, the BN power becomes greater due to interference increase. When $T_C \approx 10^{-10}$ s, the SNR has a peak. In the pulse width range of 10^{-10} s

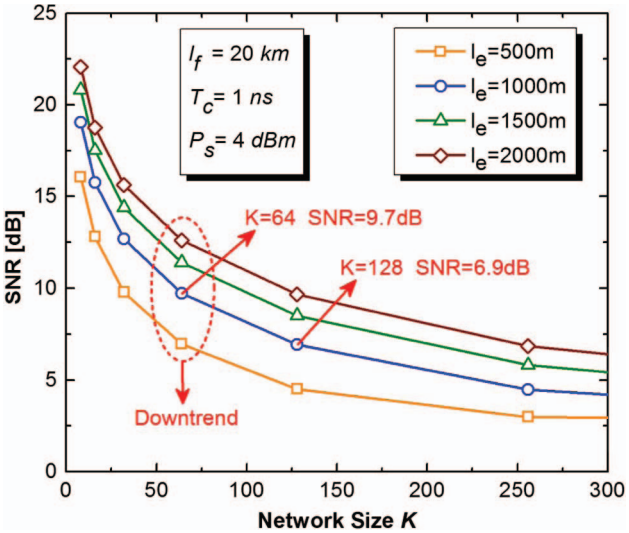

Fig. 5. SNR versus network size K.

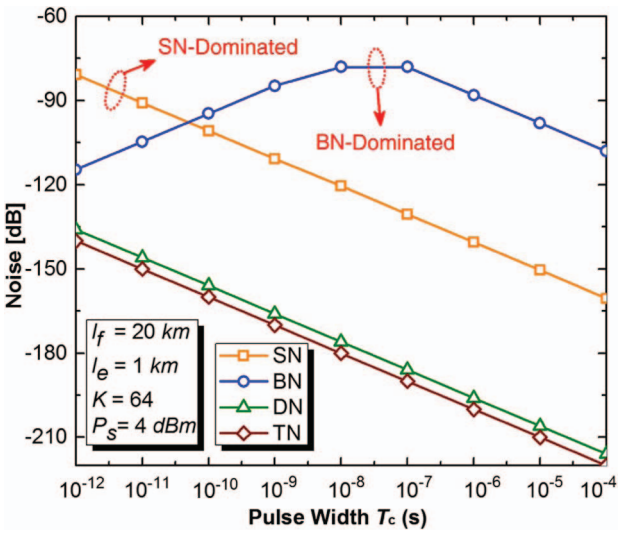

Fig. 6. Different noises versus the transmitted pulse width T_C.

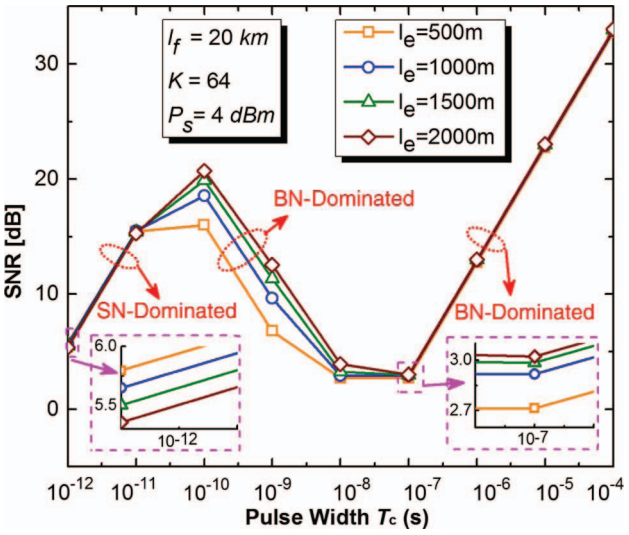

Fig. 7. SNR versus the transmitted pulse width T_C.

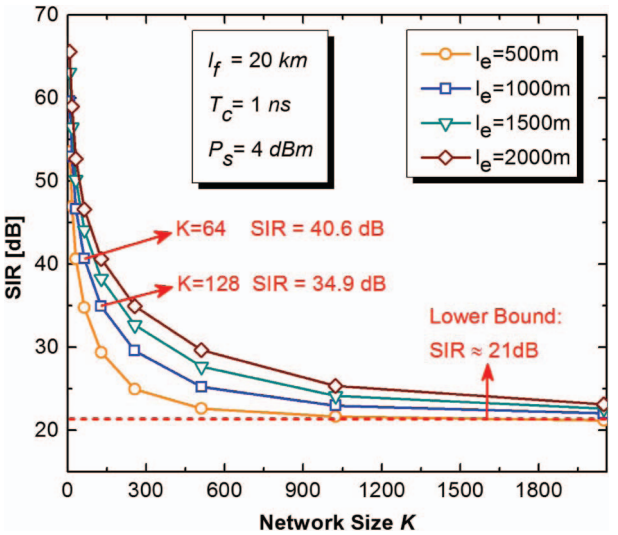

Fig. 8. SIR versus different network size K.

$< T_C < 10^{-7}$ s, the total noise power is dominated by the BN and we find the SNR on a decreasing trend. In this case, some SNR curves become separated. As the l_e increases, the SNR value gets higher. Similarly, when T_C is roughly between 10^{-8} and 10^{-7}, the SNR reaches minimum value because the BN reaches a maximum as illustrated in Fig. 6. As the T_C continues to increase, it can be observed that the SNR increases again. When $T_C > 10^{-6}$ s, although the SNR becomes improved gradually, the interference gets maximum value and the SIR reaches its low bound (this will be discussed in Fig. 9). Therefore, from Figs. 6 and 7, we can conclude that the ideal SNR would be realized when the pulse width 10^{-10} s $< T_C < 10^{-9}$ s.

C. SIR With Partial Interference

Figure 8 illustrates the SIR performance versus the network size K with different client separation distance l_e, by using $l_f = 20$ km, $K = 64$, $P_s = 4$ dBm, and values in Table III. We obtain higher SIR value when the network size K is small, due to the lesser interferences. It can be observed that the 2D coding-monitoring scheme can support the monitoring of 64 clients ($l_e = 1000$ m) with a SIR of 40.6 dB. For 128 clients, the SIR decreased to 34.9 dB due to the increase of the interference. As the network size K increases, the SIR curves gradually go to a steady value of ~21 dB because all branches have contributed the maximum μ_{int}. For a given network size (i.e., $K = 64$), as the branch maximum distance l_e increases, the SIR performance can improve because the interferences would decrease.

In Fig. 9, we study the effect of different pulse width on the SIR with $K = 64$ and $K = 256$. From the correlation distance definition just given, l_{CD} is proportional to the pulse width T_C ($l_{\text{CD}} = cFT_C/2$). Reducing T_C directly would reduce the l_{CD}, which consequently reduces the interferences. Therefore, in the part of the narrower T_C, the SIR value is relatively higher and linearly decreases as the

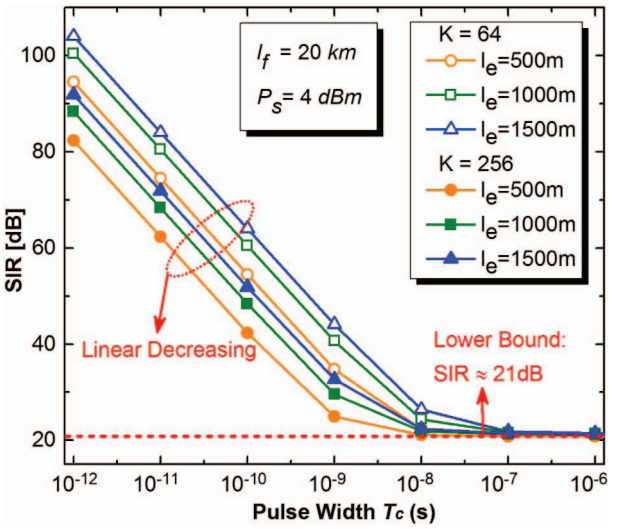

Fig. 9. SIR versus different transmitted pulse width T_c.

pulse width T_C increases. When T_C reaches 10^{-7} s, we also observe that the SIR curve decreases to a steady value of ~21 dB, because the interferences deteriorate to the maximum μ_{int}. In practice, T_C cannot be too narrow because reducing the pulse width generally reduces the total launched power and causes harm to the SNR (see Fig. 4). A proper value for T_C should be chosen to facilitate better system performance in terms of SNR and SIR. In our simulations, the optimal pulse width T_C is set to 1 ns to trade off the detection noises and the interference.

D. Relationship Between Noise and Interference

Figure 10 shows the relative relationship between SIR and SNR (i.e., the ratio between noise and interference) under different client separation distance l_e and different

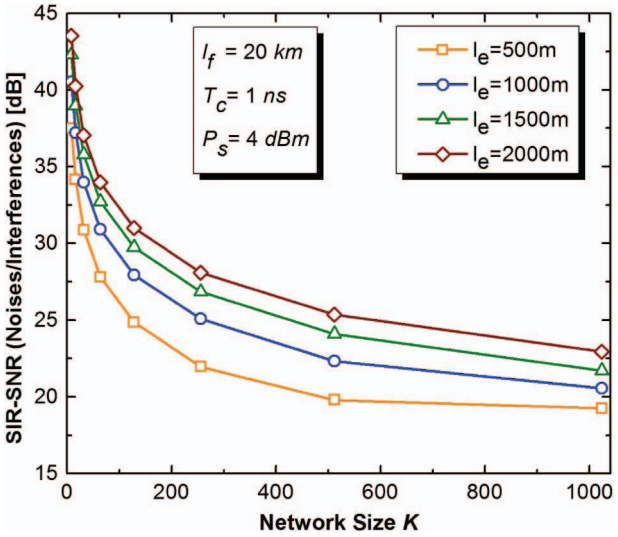

Fig. 10. The ratio between SIR and SNR with different K.

network size K by taking the values in Table III, $l_f = 20$ km, $K = 64$, and $P_s = 4$ dBm, into consideration. We can observe that SIR is much greater than SNR, i.e., the interference term is much smaller than the noise term.

Using the same simulation conditions, we also plot the ratio relationship between SIR and SNR in the cases of different transmitted pulse widths and different client separation distance l_e in Fig. 11. Similarly, it has been found that SIR is much greater than SNR. When $T_C > 10^{-7}$ s, the ratio linearly decreases because the SIR reaches a lower bound and the SNR is a linearly increasing function of the pulse width, as shown in Fig. 7. Hence, the noise term mainly dominates the performance of the monitoring system. In practice, choosing a better PD with excellent suppression noise performance is necessary.

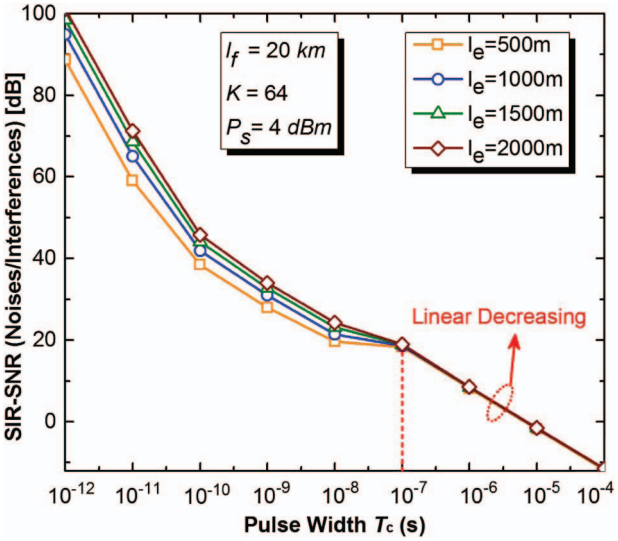

Fig. 11. The ratio between SIR and SNR with different T_C.

E. Optimal Decision Probability

To facilitate comparison using unified evaluation criteria, we define the range of $P_{\mathrm{ODP}} = (P_D - P_{\mathrm{FA}}) \geq 0.95$ to be optimal decision. We first plot ODP versus different client separation distance in Fig. 12. It can be observed that, as the client separation distance l_e increases, the ODP value becomes improved. This is because the SNR and SIR performances become improved as the client separation distance increases, as shown in Figs. 5 and 8. When $l_e = 100$ m or 500 m, the normalized threshold current (NTC) range in the optimal decision part is 0 and $0.05 < i < 0.25$, respectively. With the increase of the l_e value, the NTC range in the optimal decision part gets wider, which indicates that the optimal decision is easier to realize.

In Fig. 13, we study the effect of different network sizes K on the ODP performance for a given client separation distance (i.e., $l_e = 1000$ m). For larger network sizes ($K \geq 256$), the optimal decision could not be achieved

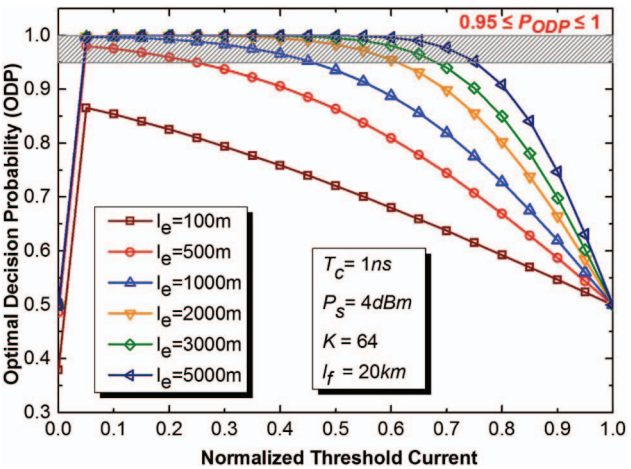

Fig. 12. ODP versus different client separation distance.

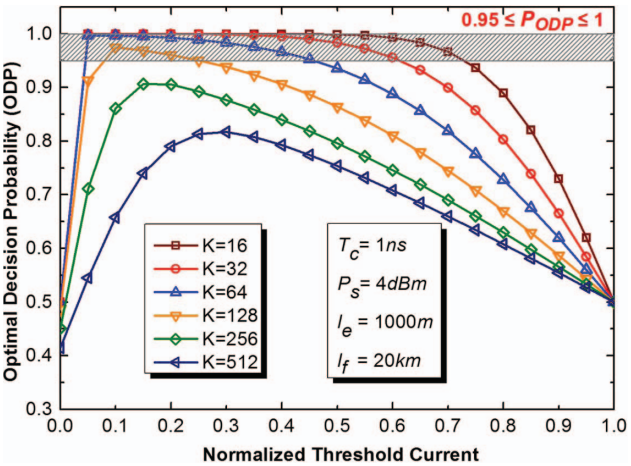

Fig. 13. ODP versus network size.

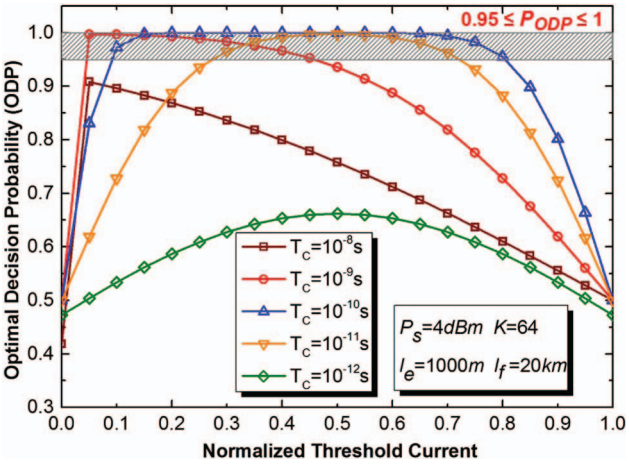

Fig. 14. ODP versus transmitted pulse width.

because the SNR and SIR are lower (see Figs. 5 and 8). As network size decreases from 128 to 16, the NTC range in the optimal decision part becomes wider due to the decreased noise and interferences.

Figure 14 shows the ODP versus different pulse width T_C. We can observe that, when T_C is between 10^{-11} s and 10^{-9} s, the optimal decision could be feasible because the SNR is relatively higher (see Fig. 7). But the ODP corresponds to the different NTC range under the different values of T_C. For $T_C > 10^{-9}$ s or $T_C < 10^{-11}$ s, the decision probability deteriorates so as to disable the optimal decision. Hence, the pulse width can be optimized depending on the network size and decision probability.

Figure 15 depicts the ODP performance with the different transmitted power; it can be observed that when the transmitted power $P_s \geq 10^{-2}$ W, the decision probability curves are the same. It should be noted that the fiber nonlinearity limits the higher transmitted pulse power in the monitoring system. For $P_s = 10^{-5}$ W, the monitoring system performance becomes very poor even for small

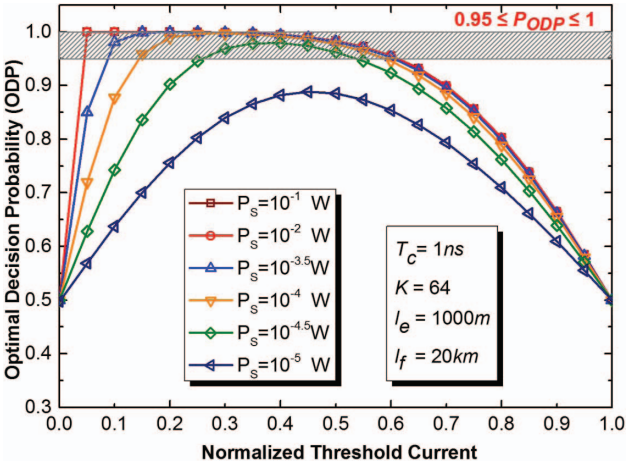

Fig. 15. ODP versus transmitted pulse power.

network sizes ($K = 64$) due to the lower pulse power and the resulting lower SNR, as shown in Fig. 4. So the optimized transmitted power can be chosen carefully to facilitate the optimal decision.

V. Conclusion

In this paper, we theoretically analyze the performance of the 2D coding-monitoring scheme in PONs by developing a mathematical model. In the model, we derive the system response function with a modularization analysis approach, and obtain the partial interference probability, SNR, and SIR. We also obtain the new expression for P_D (detection probability) and P_{FA} (false-alarm probability), which are used to find the optimal decision probability. In simulations, we investigate the impact of the different values of the network sizes, the client separation distances, the transmitted pulse width, and the transmitted pulse powers on the SNR and SIR and the relationship between them. The optimal system parameters can be chosen by jointly considering the SNR and SIR performance in a real application. These optimal system variables help to facilitate the optimal decision in practice, which hence reduces the overall cost of the monitoring system and increases the efficiency of fiber-fault identification in PONs.

Acknowledgment

The work was jointly supported by the National Natural Science Foundation of China (NSFC) (61401087), the Natural Science Foundation of Jiangsu Province (BK20140642), and the Teaching & Research Award Fund for Outstanding Young Teachers in Southeast University (2242015R30011).

References

[1] D. Nesset, "NG-PON2 technology and standards," *J. Lightwave Technol.*, vol. 33, no. 5, pp. 1136–1143, Mar. 2015.

[2] A. Fernández and N. Stol, "Influence of software and hardware failures with imperfect fault coverage on PONs OPEX," in *Optical Network Design and Modeling (ONDM)*, 2015, pp. 28–33.

[3] M. M. Rad, K. Fouli, H. A. Fathallah, L. A. Rusch, and M. Maier, "Passive optical network monitoring: Challenges and requirements," *IEEE Commun. Mag.*, vol. 49, no. 2, pp. S45–S52, Feb. 2011.

[4] Z. Liu, M. Li, and C. Chan, "Fault localization in passive optical networks using OTDR trace correlation analysis," in *Optical Fiber Communication Conf. and the Nat. Fiber Optic Engineers Conf. (OFC/NFOEC)*, 2012, paper OTu1H.2.

[5] L. Y. Herrera, G. C. Amaral, and J. P. von der Weid, "Ultra-high-resolution tunable PC-OTDR for PON monitoring in avionics," in *Optical Fiber Communication Conf. and the Nat. Fiber Optic Engineers Conf. (OFC/NFOEC)*, 2015, paper W2A.39.

[6] N. Honda, D. Iida, H. Izumita, and Y. Azuma, "In-service line monitoring system in PONs using 1650 nm Brillouin OTDR and fibers with individually assigned BFSs," *J. Lightwave Technol.*, vol. 27, no. 20, pp. 4575–4582, Oct. 2009.

[7] G. P. Temporao, G. V. Faria, P. J. Urban, and J. P. Weid, "Fault location in passive optical networks using T-OTDR and wavelength-selective isolators," in *Optical Fiber Communication Conf. and the Nat. Fiber Optic Engineers Conf. (OFC/NFOEC)*, 2013, paper NM2L.4.

[8] M. M. Rad, H. Fathallah, S. LaRochelle, and L. A. Rusch, "Computationally efficient monitoring of PON fiber link quality using periodic coding," *J. Opt. Commun. Netw.*, vol. 3, no. 1, pp. 77–86, Jan. 2011.

[9] H. Fathallah, M. M. Rad, H. Fathalla, and L. A. Rusch, "PON monitoring: Periodic encoders with low capital and operational cost," *IEEE Photon. Technol. Lett.*, vol. 20, no. 24, pp. 2039–2041, Dec. 2008.

[10] X. Zhou and X. Sun, "A centralized optical monitoring for high capacity TDM-PON based on optical frequency hopping/periodic code," in *Optical Fiber Communication Conf. and the Nat. Fiber Optic Engineers Conf. (OFC/NFOEC)*, 2012, paper JTh2A.29.

[11] X. Zhou, F. D. Zhang, and X. Sun, "Centralized PON monitoring scheme based on optical coding," *IEEE Photon. Technol. Lett.*, vol. 25, no. 9, pp. 795–797, May 2013.

[12] W. C. Kwong and G. Yang, *Optical Coding Theory With Prime.* CRC Press, 2013.

[13] G. C. Yang and W. C. Kwong, "Performance comparison of multiwavelength CDMA and WDMA+CDMA for fiber-optic networks," *IEEE Trans. Commun.*, vol. 45, no. 11, pp. 1426–1434, Nov. 1997.

[14] H. M. Kwon, "Optical orthogonal code division multiple access system Part I: APD noise and thermal noise," *IEEE Trans. Commun.*, vol. 42, no. 7, pp. 2470–2479, July 1994.

[15] T. M. Bazan, D. Harle, and I. Andonovic, "Mitigation of beat noise in time-wavelength optical code division multiple access," *IEEE J. Lightwave Technol.*, vol. 24, no. 11, pp. 4215–4222, Dec. 2006.

[16] X. Wang and K. Kitayama, "Analysis of beat noise in coherent and incoherent time spreading OCDMA," *IEEE J. Lightwave Technol.*, vol. 22, no. 10, pp. 2226–2235, Oct. 2004.

[17] M. M. Rad, H. Fathallah, and L. A. Rusch, "Performance analysis of fiber fault PON monitoring using optical coding: SNIR, SNR, and false-alarm probability," *IEEE. Trans. Commun.*, vol. 58, no. 4, pp. 1182–1192, Apr. 2010.

Min Zhu received a double Ph.D. degree from the Ecole Normale Superieure de Cachan, France, and Shanghai Jiao Tong University, China, in 2012. From 2011 to 2013, he worked as a research fellow at Nanyang Technological University, Singapore. In 2013, he joined the Department of Electronic Engineering, Southeast University, where he is currently an Associate Professor. His research interests include optical access networks and systems, optical grid, network resource scheduling, and optimization algorithms.

Jiao Zhang received a B.S. degree with a double major in measurement and control technology and instrumentation as well as computer science and technology from Yantai University, China, in 2011. Currently, he is working towards a Master's degree in the National Research Center for Optical Sensing/Communications Integrated Networking, Southeast University, China. His current research interests focus on PON monitoring and protection. He is currently a Student Member of IEEE and OSA.

Dongpeng Wang received a B.S. degree in electronic science from Huaqiao University, China, in 2013. He is currently working towards a Master's degree in the School of Electronic Science and Engineering, Southeast University, China. His research interests include performance of ROADM architecture on optical networks.

Xiaohan Sun has been a Professor of Electronics Engineering at Southeast University, Nanjing, China, since 1994. She was a Visiting Professor with the Research Laboratory of Electronics, Massachusetts Institute of Technology, Cambridge, MA, from 2002 to 2004. Her current research interests include optical sensing, communications, and networking, including high-speed optical communications systems and optical networks; photonic integration and signal processing; designing, testing, and packaging for photonics integrated circuits; and optical sensing technology.